Volume 25
Number 6
14 February 2023
Pages 4363–5294

# PCCP

Physical Chemistry Chemical Physics

rsc.li/pccp

ISSN 1463-9076

ROYAL SOCIETY OF CHEMISTRY

**PAPER**

Otto Dopfer, Shun-ichi Ishiuchi, Masaaki Fujii *et al.*
Hydration-induced protomer switching in *p*-aminobenzoic acid studied by cold double ion trap infrared spectroscopy

PCCP

ROYAL SOCIETY OF CHEMISTRY

PAPER

View Article Online
View Journal | View Issue



Cite this: *Phys. Chem. Chem. Phys.*, 2023, **25**, 4481

# Hydration-induced protomer switching in *p*-aminobenzoic acid studied by cold double ion trap infrared spectroscopy†

Kyota Akasaka,[ab] Keisuke Hirata,[acd] Fuad Haddad,[e] Otto Dopfer,*[de] Shun-ichi Ishiuchi*[acd] and Masaaki Fujii*[abd]

*Para*-Aminobenzoic acid (PABA) is a benchmark molecule to study solvent-induced proton site switching. Protonation of the carboxy and amino groups of PABA generates O- and N-protomers of $PABAH^+$, respectively. Ion mobility mass spectrometry (IMS) and infrared photodissociation (IRPD) studies have claimed that the O-protomer most stable in the gas phase is converted to the N-protomer most stable in solution upon hydration with six water molecules in the gas-phase cluster. However, the threshold size has remained ambiguous because the arrival time distributions in the IMS experiments exhibit multiple peaks. On the other hand, IRPD spectroscopy could not detect the N-protomer for smaller hydrated clusters because of broad background due to annealing required to reduce kinetic trapping. Herein, we report the threshold size for O → N protomer switching without ambiguity using IR spectroscopy in a double ion trap spectrometer from 1300 to 1800 $cm^{-1}$. The pure O-protomer is prepared by electrospray, and size-specific hydrated clusters are formed in a reaction ion trap. The resulting clusters are transferred into a second cryogenic ion trap and the distribution of O- and N-protomers is determined by mid-IR spectroscopy without broadening. The threshold to promote O → N protomer switching is indeed five water molecules. It is smaller than the value reported previously, and as a result, its pentahydrated structure does not support the Grotthuss mechanism proposed previously. The extent of O → N proton transfer is evaluated by collision-assisted stripping IR spectroscopy, and the N-protomer population increases with the number of water molecules. This result is consistent with the dominant population of the N-protomer in aqueous solution.

Received 27th September 2022,
Accepted 3rd December 2022

DOI: 10.1039/d2cp04497h

rsc.li/pccp



## 1. Introduction

Protonation is one of the most fundamental chemical reactions and a basic step in many synthetic and catalytic processes. Determining the protonation site is important because it changes the chemical properties of the molecule, such as redox behaviour, optical activity, and hydrophobicity.[1–4] In addition, some molecules vary their preferred protonation site depending on the surrounding environment such as solvent or counter ion.[5–29] Such protonation site-switching obviously has a huge effect on the chemical reactivity and biological activity of the molecule.[12,28]

Para-aminobenzoic acid (PABA) is a benchmark molecule for protonation site-switching.[8–11,13–18,20–22,29] PABA has two low-energy protonated isomers, namely the O- and N-protomers resulting from protonation of the carboxy and amino groups, respectively (Fig. 1). Their relative stability varies with type and degree of solvation. While the O-protomer is most stable in the gas phase, the N-protomer becomes more stable in polar solvents such as water. The high stability of the O-protomer in the gas phase arises from the conjugated π-electron system extending from the neutral amino group to the protonated carboxy group. On the other hand, the N-protomer becomes preferable in polar solvents due to its larger solvation energy.[14]

Infrared (IR) spectroscopy and ion mobility mass spectrometry (IMS) have previously been used to identify the protonation site in polyhydrated clusters of $PABAH^+$. Hebert and Russel

[a] *Laboratory for Chemistry and Life Science, Institute of Innovative Research, Tokyo Institute of Technology, 4259 Nagatsuta-cho, Midori-ku, Yokohama226-8503, Japan. E-mail: ishiuchi.s.aa@m.titech.ac.jp, mfujii@res.titech.ac.jp*
[b] *School of Life Science and Technology, Tokyo Institute of Technology, 4259 Nagatsuta-cho, Midori-ku, Yokohama, Kanagawa, 226-8503, Japan*
[c] *Department of Chemistry, School of Science, Tokyo Institute of Technology, 2-12-1 Ookayama, Meguro-ku, Tokyo 152-8550, Japan*
[d] *International Research Frontiers Initiative, Tokyo Institute of Technology, 4259 Nagatsuta-cho, Midori-ku, Yokohama, 226-8503, Japan. E-mail: dopfer@physik.tu-berlin.de*
[e] *Institut für Optik und Atomare Physik, Technische Universität Berlin, Hardenbergstrasse 36, 10623 Berlin, Germany*

† Electronic supplementary information (ESI) available. See DOI: https://doi.org/10.1039/d2cp04497h

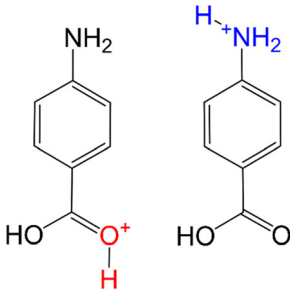


Fig. 1 Molecular structure of O- and N-protomers of $PABAH^+$.

tracked changes in the protonation positions in $PABAH^+(H_2O)_n$ by low-temperature IMS.[30] They used the electrospray source with a mixed solvent of acetonitrile and water to generate simultaneously both O- and N-protomers. Both protomers are clearly separated by the arrival time distribution (ATD) of the monomer. For clusters up to $n$ = 4, they fitted two Gaussian functions to the ATD but changed to a single broader Gaussian function for $n$ = 5 and a narrower Gaussian for $n$ = 6. From these results, they concluded that the protomer population is dominated by the N-protomer at $n$ = 6. To rationalize this result, they proposed a Grotthus mechanism for proton transfer along a water bridge between the $NH_2$ and COOH groups at $n$ = 6. However, the ATD exhibit for all hydrated $PABAH^+$ clusters multiple peaks and fitting these by only one or two Gaussians may not be fully appropriate, although the DFT calculations also show that the N-protomer becomes most stable at $n$ = 6.

In contrast to the less structure-sensitive IMS spectra, IR spectroscopy can provide direct evidence for the structural assignments of the O- and N-protomers. To this end, Williams and co-workers measured the IR photodissociation (IRPD) spectra of $PABAH^+(H_2O)_n$ ($n$ = 1–6) in the OH/NH stretch range (2600–3900 $cm^{-1}$) to determine how many water molecules are necessary to stabilize the N-protomer.[10] They introduced $PABAH^+(H_2O)_n$ clusters generated directly in the electrospray source into the ion cyclotron resonance mass spectrometer and measured their IRPD spectra. It is known that the electrospray of PABA with water solvent selectively generates the O-protomer of the $PABAH^+$ monomer. The IRPD spectra of $PABAH^+(H_2O)_n$ ($n$ = 1–5) give free NH stretching bands similar to the monomer, while new vibrational bands appear with high intensity in the spectrum of $n$ = 6 (although such bands are already weakly present also for $n < 6$). They assigned the new bands to the N-protomer in the hydrated cluster, and concluded that hydration by six water molecules stabilizes the N-protomer such that the preferred protonation site switches from COOH to $NH_2$ in $PABAH^+$ at $n$ = 6. One problem of this approach is kinetic trapping of the N-protomer in the hydrated cluster in the electrospray process. As the N-protomer is more stable in aqueous solution, it may remain in the hydrated clusters generated in the electrospray source regardless of its relative stability. To avoid the kinetically trapped N-protomer, they carefully annealed the hydrated clusters by collisions with $N_2$ and measured the IRPD spectra at 130 K. Although annealing and the measurement at 130 K were assumed to avoid kinetic trapping, all IRPD spectra became broader and the spectral signatures of the two protomers became less resolved. Consequently, the presence of the N-protomer in the $n$ = 1–5 spectra is not clear because of the broad background, as stated by the authors. In summary, it appears clear that hydration by six water molecules is sufficient to induce O → N protonation site-switching, however, the minimal number of water molecules required to promote the switching is still unclear.

To reliably determine the threshold for hydration-induced O → N protonation site-switching, we apply herein a more sophisticated spectroscopic strategy. It has clearly been established that only the O-protomer is produced when the $PABAH^+$ monomer is generated from the electrospray of a slightly acidic protic solution.[12] This O-protomer of the $PABAH^+$ monomer is mass-selected and then introduced into the first ion trap (reaction trap[31,32]) containing water vapour to grow $PABAH^+(H_2O)_n$ clusters. If then the N-protomer is detected in the hydrated clusters after the first ion trap by IRPD, it is without any doubt the result of O→N protonation site-switching. The reaction trap has to be kept at a certain elevated temperature (80 K in this work) to promote the intracluster proton transfer reaction. If we measure the IR spectra under such conditions, spectral broadening may not be avoided. This problem is solved by the following means. We use one more ion trap[33–35] at very low temperature (4 K in this work) and the hydrated clusters in the warmer reaction trap are mass-selected and transferred into the cryogenic second ion trap at a frozen N/O population ratio. Then, we measure the population of the O- and N-protomers using IRPD spectroscopy by irradiating the mass-selected clusters with a tuneable IR laser (using the tagging approach[36]). The broadening of IR spectra can be avoided because of the low temperature. In addition, we expand the spectral range down to mid-IR to readily distinguish between the O- and N-protomers. Recently, Johnson and coworkers reported the IRPD spectra of the O- and N-protomers of the $PABAH^+$ monomer and found the clear discrimination of both monomers by probing the C=O stretching range (the C=O band can occur only for the N-protomer).[20] In addition, the shape of the C=O stretching band is rather insensitive to H-bonding with water molecules. This is in stark contrast to the previously investigated N–H stretching range, and thus the new IRPD spectra recorded in the mid-IR (6 μm) range will give clear evidence for the protomer assignments. Finally, we also apply the recently developed collision-assisted stripping IR spectroscopic technique (CAS-IR),[27] which enables us to precisely determine the protomer population in highly hydrated clusters. By using both IRPD and CAS-IR in the double ion trap spectrometer, we examine how the protomer abundance ratio in $PABAH^+$ changes as the number of water molecules increases.

## 2. Experimental and computational methods

A methanol solution of PABA (Wako, $10^{-5}$ M) with 0.5% of formic acid is electrosprayed and the fine droplets are

 

desolvated in a glass capillary heated to ~80 °C. The generated ions are introduced into the vacuum *via* an ion funnel. The ions of interest are mass-selected by a quadrupole mass spectrometer (QMS) and transported by a tapered hexapole ion guide. The ions are hydrated in an octupole ion trap (reaction trap[31,32]) with water vapour introduced by a pulsed valve. The temperature of the reaction trap is maintained at 80 K. Hydrated ions are mass-selected in the second QMS and introduced into the cryogenic quadrupole ion trap (QIT[37]) *via* a quadrupole ion deflector and an octupole ion guide. The QIT is maintained at 4 K by a closed-cycle two-stage He refrigerator. Helium buffer gas mixed with $H_2$ is introduced into the QIT by a pulsed valve for collisional cooling of hydrated ions down to ~10 K, and subsequently $H_2$ molecules are attached to the hydrated $PABAH^+$ cluster ($H_2$ tagging method[36]). The cold hydrated ions, $PABAH^+(H_2O)_n(H_2)_m$, are irradiated with a tuneable OPO/OPA IR laser. The $PABAH^+(H_2O)_n$ photofragments produced by the dissociation of all $H_2$ molecules are monitored by a time-of-flight mass spectrometer. $H_2$ is weakly bound so that the structure of the hydrated $PABAH^+(H_2O)_n$ clusters are not perturbed.[36] All IRPD spectra are measured by monitoring the fragment ion yield generated by $H_2$ dissociation as a function of laser wavenumber.

When CAS-IR spectra are measured, hydrated ions are directed into the QIT with high kinetic energy (~16 eV) by lowering the offset voltage at the QIT entrance electrode. The ions are then collisionally dissociated to bare $PABAH^+$, and $H_2$ molecules are attached to $PABAH^+$. The $H_2$-detached photofragments are detected by scanning the wavenumber of the IR laser.

Molecular structures and vibrational frequencies of $PABAH^+(H_2O)_n$ are calculated by density functional theory (DFT). The initial structures of $PABAH^+(H_2O)_n$ are generated automatically by the OPLS[38] force field implemented in MacroModel.[39] Preliminary DFT calculations are performed for the initial structures at the dispersion-corrected ωB97X-D/6-31G(d,p) level using the Gaussian16[40] software. The ωB97X-D method gives better results than B3LYP and MP2.[10,27] Relative Gibbs free energies at 298.15 K are also calculated at the same level. The structures whose relative Gibbs free energy are within 10 kJ $mol^{-1}$ of the most stable protomer are re-calculated at the higher ωB97X-D/6-311++G(d,p) level[27] (ESI†). All calculated conformers displayed are local minima on the potential energy surface. The harmonic vibrational frequencies obtained are scaled by 0.952 in the 3 μm range[27] and 0.970 (O-protomer)/0.955 (N-protomer) in the 6 μm range. The scaling factor for the 6 μm range is determined by the characteristic band for each protomer at $n$ = 0 (Fig. S1, ESI†). In addition, the Gibbs free energies are re-calculated at 80 K at the higher computational level (Tables S1–S8, ESI†).

## 3. Results and discussion

Fig. 2 shows the IRPD spectra of $PABAH^+(H_2O)_{n\leq 7}$ recorded in the 1300–1800 $cm^{-1}$ range. Based on previous studies of bare $PABAH^+$,[20] the bands observed in the IRPD spectrum are assigned to $C(OH)_2^{asym}$ at 1508 $cm^{-1}$, $C–NH_2^{aryl}$ at 1519 $cm^{-1}$, $C–C(OH)_2^{aryl}$ at 1570–1600 $cm^{-1}$, and $NH_2^{bend}$ at 1658 $cm^{-1}$. The

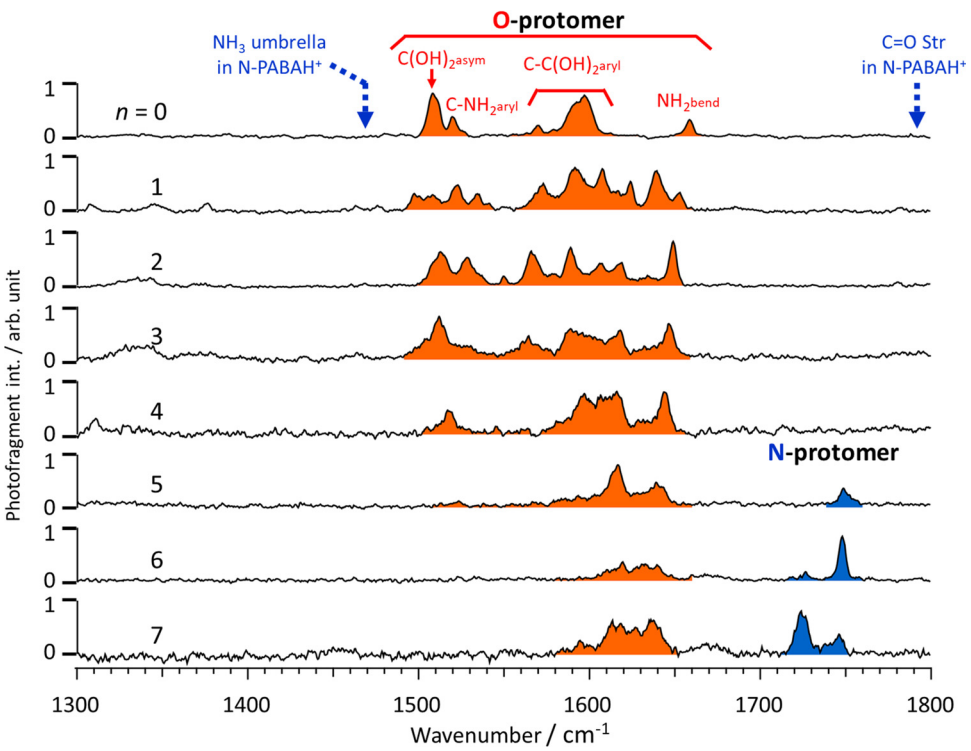


Fig. 2 IRPD spectra of $PABAH^+(H_2O)_n$ with $n$ = 0–7.

bands characteristic of the N-protomer of the $PABAH^+$ monomer, *i.e.*, the C=O stretch (1790 $cm^{-1}$) and $NH_3$ umbrella (1470 $cm^{-1}$) vibrations indicated by broken lines, are not observed in the spectrum. Thus, all bands present in the recorded spectrum of $PABAH^+$ ($n$ = 0) are attributed to the O-protomer (color-coded in red). This result indicates that the initial protomeric ion injected into the reaction trap is the most stable gas-phase ion, and kinetic trapping of the higher energy N-protomer most stable in solution is not observed. The IRPD spectra of $PABAH^+(H_2O)_n$ ($n$ = 1–7) also show the vibrational bands in the 1500–1700 $cm^{-1}$ range, which are tentatively assigned to hydrated clusters with an O-protomeric $PABAH^+$ core. The $NH_3$ umbrella band, which is the characteristic mode of the N-$PABAH^+$ core, will be shifted in its hydrated clusters because of H-bonding (NH···O ionic H-bonds). On the other hand, the C=O stretch band is relatively insensitive to hydration because water molecules form H-bonds mainly around the positively charged $NH_3^+$ centre. Thus, the absence and presence of a band above 1700 $cm^{-1}$ can be attributed to the O- and N-protomer, respectively. This argument means that only O-protomers are populated in the hydrated $PABAH^+(H_2O)_n$ up to four water molecules. For the hydrated cluster with five water molecules, a new band is observed in the range above 1700 $cm^{-1}$. This band at 1748 $cm^{-1}$ is assigned to the C=O stretch of the N-protomeric core, and thus strongly suggests that the hydration by five water molecules makes the N-protomer of $PABAH^+$ stable enough to be detected. Similarly, the IRPD spectra of hydrated clusters with six and seven water molecules show vibrational bands in the range above 1700 $cm^{-1}$ (1726 and 1748 $cm^{-1}$, 1725 and 1746 $cm^{-1}$, respectively). Thus, O- and N-protomers coexist in the $PABAH^+(H_2O)_{5-7}$ size range.

To confirm the presence of the N-protomer, theoretical spectra of O- and N-protomers in $PABAH^+$-$(H_2O)_n$ ($n$ = 0–7) obtained by quantum chemical calculations are compared to the observed spectra. Gibbs free energies of optimized structures for $n$ = 0–7 are listed in Tables S1–S8 in ESI,† respectively. The computed spectra of the ten most stable structures for $n$ = 0–3 are compared to the observed ones in Fig. S2–S5 (ESI†), respectively. The bands observed for $n$ = 0–3 are well assigned to O-protomer transitions (Fig. S2–S5, ESI†). Fig. 3b compares the computed spectra of the most stable N- and O-protonated $PABAH^+(H_2O)_4$ clusters to the observed IRPD spectrum (Fig. 3a). The bands observed between 1500 and 1650 $cm^{-1}$ are similar to those in the spectrum computed for the most stable O-protomer in $PABAH^+(H_2O)_4$. The theoretical spectra for the N-protomer predict the C=O stretch band at 1765 $cm^{-1}$. However, no clear band is observed in the range above 1700 $cm^{-1}$, suggesting that the population of the N-protomer in $PABAH^+(H_2O)_4$ is (at most) small and thus below the

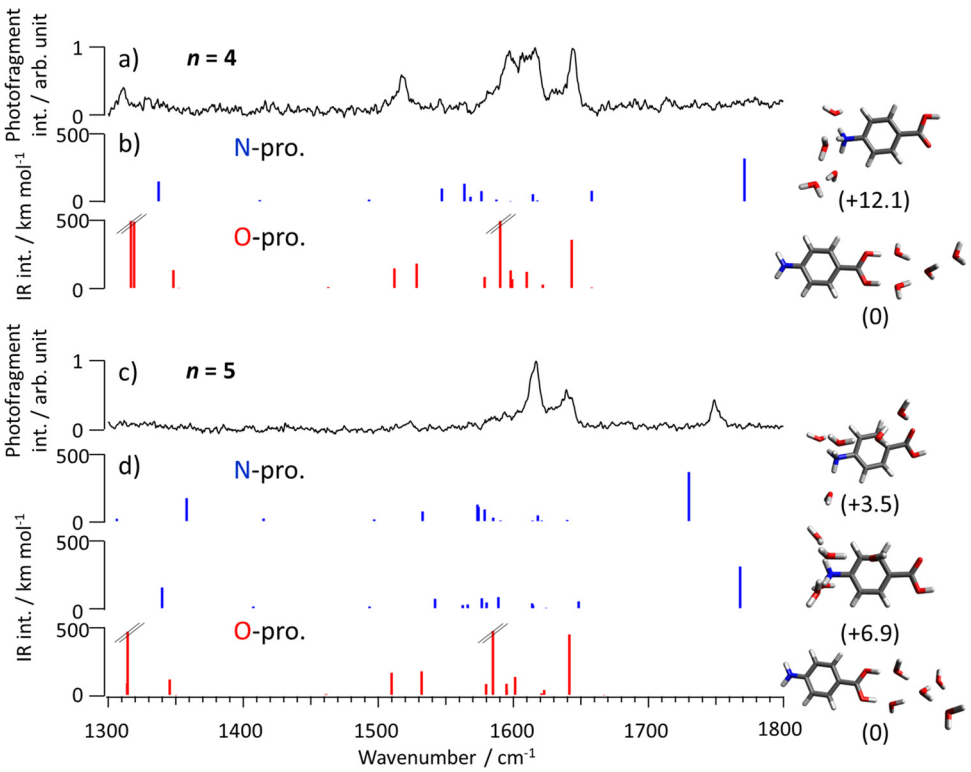


Fig. 3 IRPD spectrum of $PABAH^+(H_2O)_n$ with (a) $n$ = 4 and (c) $n$ = 5 in comparison with (b,d) theoretical IR spectra of the most stable N- and O-protomers. Molecular structures are shown next to the computed IR spectra with their relative Gibbs free energies at 80 K in parentheses (in kJ $mol^{-1}$). It should be noted that the detection sensitivity decreases toward the lower frequency range because of the lower dissociation efficiency of $H_2$-tagged molecules.[45] Calculated intensities of the bands at 1316, 1318, and 1589 $cm^{-1}$ in the $n$ = 4 cluster of the O-protomer core and 1314 and 1584 $cm^{-1}$ in the $n$ = 5 cluster of the O-protomer core are 711, 734, 896, 1392, and 863 km $mol^{-1}$, respectively.

 

detection limit (Fig. S6–S9, ESI†). This observation is indeed consistent with the calculated Gibbs free energies (80 K) of $PABAH^+(H_2O)_4$, for which the most stable isomer with an N-protomer core is less stable than the most stable one with an O-protomer core by 12.1 kJ $mol^{-1}$. It should be noted that the $NH_3$ umbrella band for $n$ = 4 is blue-shifted by ~90 $cm^{-1}$ (frequency: 1547 $cm^{-1}$, IR intensity: 114 km $mol^{-1}$) and overlaps with bands of the O-protomer, making this vibration insensitive for protomer assignment.

In contrast to $n \leq 4$, the IRPD spectrum of $PABAH^+(H_2O)_5$ is not solely assigned to the O-protomer. Specifically, the band at 1748 $cm^{-1}$ cannot be reproduced by O-protomers (Fig. S10 and S12, ESI†). In contrast, one of the theoretical IR spectra of the two most stable pentahydrated $PABAH^+$ clusters with an N-protomer core, for which the C=O stretches are calculated at 1730 and 1768 $cm^{-1}$ (Fig. 3d), can explain the band at 1748 $cm^{-1}$ (Fig. 3c, d and Fig. S11, S13, ESI†). A more detailed isomer assignment for $n$ = 5 will be given below after assigning the spectra for $n$ = 6 and 7. In any case, the observed band at 1748 $cm^{-1}$ is a clear signature of the N-protomer core in pentahydrated $PABAH^+$. Bands around 1630 $cm^{-1}$ are attributed to the most stable O-protomer in pentahydrated clusters. The observation of N-protomer clusters at $n$ = 5 is consistent with their significant stabilization in Gibbs free energy relative to the most stable O-protomer (only 3.5 and 6.9 kJ $mol^{-1}$ less stable at 80 K) by adding one more water ($n$ = 4 → 5). From this assignment, we conclude that the N-protomeric core begins to appear already at $n$ = 5 and not at $n$ = 6 under the current experimental conditions.

The coexistence of O- and N-protomers in the $PABAH^+(H_2O)_n$ clusters with $n$ = 6 and 7 is also confirmed by their IRPD spectra shown in Fig. 4a–d, respectively. In both spectra, two vibrational bands are observed in the 1700–1800 $cm^{-1}$ range, which cannot be assigned to O-protomers (Fig. 4 and Fig. S14, S16, ESI†). The most stable conformer of $PABAH^+(H_2O)_6$ has an N-protomeric core, in agreement with previous calculations.[10] The bands at 1726 and 1748 $cm^{-1}$ can be assigned to C=O stretch modes of the most stable and less stable N-protomers of $PABAH^+(H_2O)_6$ (Fig. 4a, b and Fig. S15, ESI†). The different frequencies of the two C=O stretch modes arise from the presence and absence of H-bonding to a water molecule (see corresponding structures in Fig. 4b and Fig. S17, ESI†). It should be noted that the free C=O stretching band (1748 $cm^{-1}$) in the less stable conformer is slightly red-shifted from that of bare $PABAH^+$ (1781 $cm^{-1}$) probably due to the change of electron density upon hydration of the $NH_3^+$

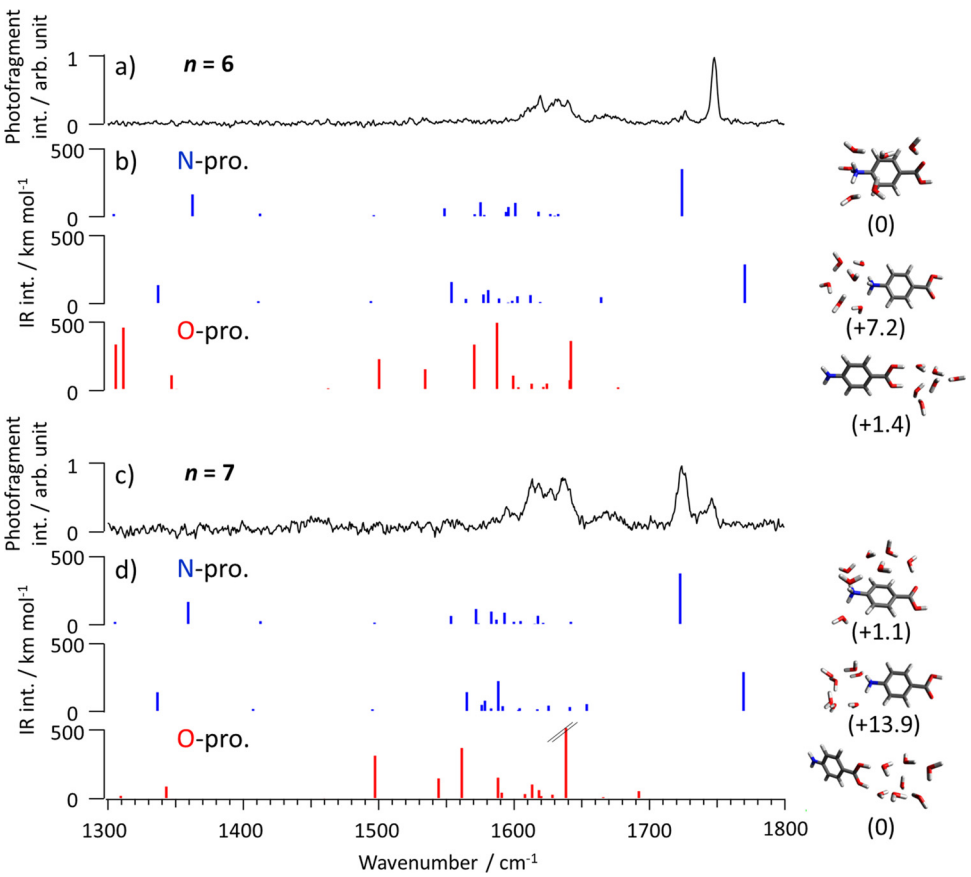


Fig. 4 IRPD spectrum $PABAH^+(H_2O)_n$ with (a) $n$ = 6 and (c) $n$ = 7 in comparison with (b and d) theoretical IR spectra of the most stable N- and O-protomers. Molecular structures are shown next to the computed IR spectra with their relative Gibbs free energies at 80 K in parentheses (in kJ $mol^{-1}$). It should be noted that the detection sensitivity decreases in the lower frequency range because of the lower dissociation efficiency of $H_2$-tagged molecules.[45] The calculated intensity of the band at 1638 $cm^{-1}$ of the O-protomer core is 686 km $mol^{-1}$.

group. We name herein the conformers with and without H-bonding between C=O and water as bridged and unbridged conformers, respectively. Similar to $n$ = 6, two C=O stretch bands appear at $n$ = 7, but their relative intensities are reversed, indicating that the preferred geometry for $n$ = 7 is a bridged conformer (Fig. 4c, d and Fig. S18–S21, ESI†). Comparing the energies of the two types of structures for each hydrated cluster, the bridged structure is more stabilized in $n$ = 7 than in $n$ = 6 (by 12.8 *vs.* 7.2 kJ mol$^{-1}$).

When we now look at the single C=O stretch band observed for $n$ = 5, it can be assigned to an unbridged conformer by comparing its frequency to those for $n$ = 6 and 7. However, this type of C=O stretch is calculated for a metastable conformer, which is 3.4 kJ mol$^{-1}$ less stable than the most stable N-protomer (Fig. 3 and Fig. S13, ESI†). A similar inconsistency is found for $n$ = 6. The higher-frequency C=O stretch band has to be assigned to the unbridged conformer which is more than 7 kJ mol$^{-1}$ less stable than the most stable bridged one (Fig. S15, ESI†), although the band of the unbridged isomer is more intense than the one of the bridged isomer. The most probable scenario is that the reaction product, the N-protomer, is thermally not equilibrated at 80 K. The produced N-protomer is probably hotter than 80 K because of exothermic intracluster O → N proton transfer. Alternatively, hot O-protomers may transiently be generated by hydration of PABAH$^+$ by converting hydration energy into internal energy. As a result, the hot O-protomer may overcome the reaction barrier for O → N proton transfer. The produced "hot" N-protomer may then be kinetically trapped in the cold reaction trap (80 K). This means that the kinetically trapped N-protomer reflects the structural information at higher temperature. Therefore, the energy gap between experiment and theory arises from a temperature effect. In fact, when we elevate the temperature from 80 to 298 K for the free energy calculations, unbridged N-protomers become more stable than bridged ones for $n$ = 5 and 6 (Fig. S22, ESI†), qualitatively consistent with the experimental IRPD spectra. The higher stability of the unbridged N-protomers at higher temperature can then be ascribed to entropy.

Although the IRPD spectra shown in Fig. 3 and 4 clearly indicate the presence/absence of the N-protomer, they do not directly reveal the population ratio of O- and N-protomers. The population ratio may be derived by normalizing the integrated experimental band intensities using the computed IR oscillator strengths, which however can vary strongly among the various conformers. The exact conformer assignments are very difficult because there are too many possible conformers predicted in the low energy range (*e.g.*, more than ten conformers are lower than 3 kJ mol$^{-1}$ for the $n$ = 6 clusters of the O-protomer core). This makes a reliable population analysis almost impossible. To avoid this problem, collision-stripping assisted IR (CAS-IR) spectroscopy has been developed and tested for a prototypical molecule, benzocaine H$^+$, an analogue of PABAH$^+$.[27] This method measures the populations of O- and N-protomers after stripping all water molecules from the protonated solute molecule and thus the conformational distributions in the hydrated clusters must not necessary be determined. Significantly, the collisional stripping does not affect the protonation position.[27] Here, we apply CAS-IR spectroscopy to PABAH$^+$(H$_2$O)$_n$ and experimentally determine the relative abundance of O- and N-protomers for each size of the hydrated clusters.

To this end, Fig. 5c shows CAS-IR spectra of PABAH$^+$(H$_2$O)$_n$ ($n$ = 0–7). After stripping the water ligands, PABAH$^+$ forms van

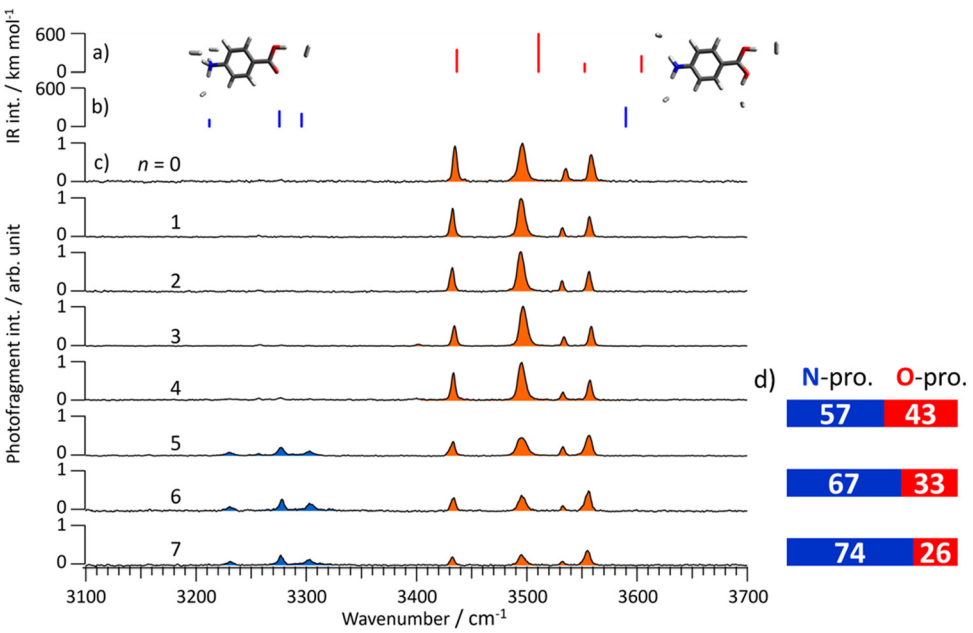


Fig. 5 Calculated IR spectra of the (a) O- and (b) N-protomers of PABAH$^+$(H$_2$)$_4$. (c) Observed CAS-IRPD spectra of PABAH$^+$(H$_2$O)$_n$ ($n$ = 0–7) and (d) estimated population ratio for N- and O-protomers for $n$ = 5–7. The calculated frequencies of the OH stretching modes are overestimated compared to the NH stretching modes.

 

der Waals complexes with $H_2$, which is introduced into the second ion trap together with the He buffer gas. Then, the IR transitions of the $PABAH^+$ monomer can be measured by loss of $H_2$ (tagging method[36]). Thus, all bands can be assigned by vibrational transitions of the monomer isomers. The spectrum for $n = 0$ shows four bands in the 3400–3600 $cm^{-1}$ range. These bands are in good agreement with the calculated spectrum of O-protonated $PABAH^+$ tagged by four $H_2$ molecules (Fig. 5 and Fig. S23, ESI†). The bands at 3435, 3496, 3535, and 3558 $cm^{-1}$ are assigned to symmetric NH stretching, outward-facing OH stretching, antisymmetric NH stretching, and OH stretching toward the benzene ring, respectively. Only these bands are observed for mono- to tetrahydrated $PABAH^+$ clusters after collisional stripping of the water ligands. Thus, $PABAH^+$ has only the O-protonated form in these clusters with one to four water molecules.

In the CAS-IR spectrum of $n = 5$, new bands appear in the range from 3200 to 3350 $cm^{-1}$. From the comparison to the theoretical IR spectra shown in Fig. 5b, these bands at 3230, 3278, and 3303 $cm^{-1}$ are assigned to symmetric and two antisymmetric stretching vibrations of the $NH_3$ group in the N-protomer tagged with four $H_2$ molecules. The theoretical spectra also predict the OH stretching vibration at 3580 $cm^{-1}$. Probably this mode corresponds to the band at 3555 $cm^{-1}$, which overlaps with the one of the OH stretching of the O-protomer, because this band appears more strongly than predicted for the O-protomer. Thus, the appearance of the bands between 3200 and 3350 $cm^{-1}$ confirms the formation of the N-protomer in the pentahydrated $PABAH^+$ cluster, as well as the interpretation of the IRPD spectra in the 6 μm range. Similarly, the coexistence of O- and N-protomers in the $PABAH^+(H_2O)_n$ with $n = 6$ and 7 is confirmed by the appearance of the bands in the 3200–3350 $cm^{-1}$ range.

The population ratio of N- and O-protomers is quantitatively estimated by normalizing the CAS-IR band intensities using the calculated IR oscillator strength of $PABAH^+$ (more exactly $H_2$-tagged $PABAH^+$). The CAS-IR intensities are obtained by fitting the CAS-IR spectra with Lorentzian profiles (details are shown in Fig. S24, ESI†). Finally, we obtain the N : O ratio of 6 : 4 for $n = 5$, 2 : 1 for $n = 6$, and 3 : 1 for $n = 7$, indicating that this ratio increases with the number of water molecules (Fig. 5d). It should be noted that the N-protomer is likely to be kinetically trapped and the N ↔ O interconversion is not thermally equilibrated. Therefore, the obtained population ratio does not reflect the thermodynamic stability but the extent of the O → N proton transfer reaction. The O → N intracluster proton transfer is more pronounced as the number of attached water ligands is increased in the cluster. This observation suggests that the reaction barrier for the proton transfer is lowered by sequential addition of water molecules.

## 4. Summary

We have applied double ion trap IRPD and CAS-IR spectroscopy to hydrated clusters of $PABAH^+$. By selective formation of the O-protomer in the electrospray source and the sequential cluster formation with water molecules in the reaction trap combined with mid-IR spectroscopy in the C=O stretch range, we have determined the threshold size for hydration-induced N-protomer formation as five water molecules, without ambiguity caused by kinetic trapping in the electrospray source. This threshold size of $n = 5$ is smaller than $n = 6$ reported by previous studies. Hebert and Russel proposed the Grotthuss mechanism for the intracluster proton transfer in the hydrated clusters of $PABAH^+$ because of the bridged structure of the hydrated N-protomer ($n = 6$) in which the $NH_3^+$ and COOH groups are connected by a H-bonded water chain.[30] However, the bridged conformer appears minor in the current IRPD spectrum for $n = 6$ and the pentahydrated N-protomer of $PABAH^+$ does not have such a bridged structure. Thus, we should consider a non-Grotthuss mechanism for the proton transfer, such as the vehicle mechanism, in this size regime.[19,41,42] On the other hand, the bridged structure becomes most abundant in higher hydrated clusters ($n = 7$). This suggests that the Grotthuss mechanism[13,26,43,44] may also be involved in the proton transfer, especially in larger hydrated clusters. However, a clear conclusion that can be drawn here for the smaller clusters ($n \leq 6$) is that if the Grotthuss mechanism plays a role in the proton transfer, it would first require the formation of energetically highly unfavourable structures. The proton transfer mechanism can be further examined in the future by hydration with heavy water ($D_2O$). Concerning the N/O protomer population, our measurements are currently limited up to the hydration with seven water molecules. It may be interesting to explore how many water molecules are required to reach a 100% population of the N-protomer as observed in solution. Another interesting aspect is the acceleration of the proton transfer reaction by raising the temperature of the reaction trap. These future plans, as well as the application of double ion trap spectroscopy[31,32] to other molecules that contain two or more protonation sites, will allow us to explore the mechanism of intracluster proton transfer in hydrated clusters and aqueous solution at the molecular level.

## Conflicts of interest

There are no conflicts to declare.

## Acknowledgements

This work was supported in part by KAKENHI (JP19K23624, JP20K20446, JP20H00372, JP21H04674, and JP21K14585), the Core-to-Core program (JPJSCCA20210004) from Japan Society for the Promotion of Science, research grant from World Research Hub Initiative (WRHI) of Tokyo Institute of Technology, the Cooperative Research Program of the ''Network Joint Research Center for Materials and Devices'' from the Ministry of Education, Culture, Sports, Science and Technology (MEXT), Japan. The computations were performed at the Research Centre for Computational Science, Okazaki, Japan. M. F. is

grateful for support from the Alexander von Humboldt foundation. O. D. acknowledges support from Deutsche Forschungsgemeinschaft (DFG, DO 729/10) and the World Research Hub Initiative (WRHI) of Tokyo Institute of Technology.

## References

1 N. Gupta and H. Linschitz, *J. Am. Chem. Soc.*, 1997, **119**, 6384–6391.
2 M. K. Nazeeruddin, S. M. Zakeeruddin, R. Humphry-Baker, M. Jirousek, P. Liska, N. Vlachopoulos, V. Shklover, C.-H. Fischer and M. Grätzel, *Inorg. Chem.*, 1999, **38**, 6298–6305.
3 C. H. Cheon and H. Yamamoto, *J. Am. Chem. Soc.*, 2008, **130**, 9246–9247.
4 J. T. Mohr, A. Y. Hong and B. M. Stoltz, *Nat. Chem.*, 2009, **1**, 359–369.
5 D. H. Aue, H. M. Webb and M. T. Bowers, *J. Am. Chem. Soc.*, 1976, **98**, 311–317.
6 N. Solcà and O. Dopfer, *Angew. Chem., Int. Ed.*, 2003, **42**, 1537–1540.
7 N. Solcà and O. Dopfer, *J. Am. Chem. Soc.*, 2004, **126**, 1716–1725.
8 Z. Tian and S. R. Kass, *Angew. Chem., Int. Ed.*, 2009, **48**, 1321–1323.
9 J. Schmidt, M. M. Meyer, I. Spector and S. R. Kass, *J. Phys. Chem. A*, 2011, **115**, 7625–7632.
10 T. M. Chang, J. S. Prell, E. R. Warrick and E. R. Williams, *J. Am. Chem. Soc.*, 2012, **134**, 15805–15813.
11 J. L. Campbell, J. C. Y. Le Blanc and B. B. Schneider, *Anal. Chem.*, 2012, **84**, 7857–7864.
12 S. Warnke, J. Seo, J. Boschmans, F. Sobott, J. H. Scrivens, C. Bleiholder, M. T. Bowers, S. Gewinner, W. Schöllkopf and K. Pagel, *et al.*, *J. Am. Chem. Soc.*, 2015, **137**, 4236–4242.
13 J. L. Campbell, A. M.-C. Yang, L. R. Melo and W. S. Hopkins, *J. Am. Soc. Mass Spectrom.*, 2016, **27**, 1277–1284.
14 J. Seo, S. Warnke, S. Gewinner, W. Schöllkopf, M. T. Bowers, K. Pagel and G. von Helden, *Phys. Chem. Chem. Phys.*, 2016, **18**, 25474–25482.
15 A. L. Patrick, A. P. Cismesia, L. F. Tesler and N. C. Polfer, *Int. J. Mass Spectrom.*, 2017, **418**, 148–155.
16 E. Matthews and C. E. H. Dessent, *Phys. Chem. Chem. Phys.*, 2017, **19**, 17434–17440.
17 H. Xia and A. B. Attygalle, *J. Mass Spectrom.*, 2018, **53**, 353–360.
18 R. Kumar and H. I. Kenttämaa, *J. Am. Soc. Mass Spectrom.*, 2020, **31**, 2210–2217.
19 K. Ohshimo, S. Miyazaki, K. Hattori and F. Misaizu, *Phys. Chem. Chem. Phys.*, 2020, **22**, 8164–8170.
20 T. Khuu, N. Yang and M. A. Johnson, *Int. J. Mass Spectrom.*, 2020, **457**, 116427.
21 P. R. Batista, T. C. Penna, L. C. Ducati and T. C. Correra, *Phys. Chem. Chem. Phys.*, 2021, **23**, 19659–19672.
22 M. Demireva and P. B. Armentrout, *J. Phys. Chem. A*, 2021, **125**, 2849–2865.
23 M. McCullagh, S. Goscinny, M. Palmer and J. Ujma, *Talanta*, 2021, **234**, 122604.
24 T. Uhlemann, G. Berden and J. Oomens, *Eur. Phys. J. D*, 2021, **75**, 23.
25 N. Takeda, K. Hirata, K. Tsuruta, G. D. Santis, S. S. Xantheas, S. Ishiuchi and M. Fujii, *Phys. Chem. Chem. Phys.*, 2022, **24**, 5786–5793.
26 B. Ucur, A. T. Maccarone, S. R. Ellis, S. J. Blanksby and A. J. Trevitt, *J. Am. Soc. Mass Spectrom.*, 2022, **33**, 347–354.
27 K. Hirata, F. Haddad, O. Dopfer, S. Ishiuchi and M. Fujii, *Phys. Chem. Chem. Phys.*, 2022, **24**, 5774–5779.
28 G. D. Santis, N. Takeda, K. Hirata, K. Tsuruta, S. Ishiuchi, S. S. Xantheas and M. Fujii, *J. Am. Chem. Soc.*, 2022, **144**, 16698–16702.
29 T. Khuu, S. J. Stropoli, K. Greis, N. Yang and M. A. Johnson, *J. Chem. Phys.*, 2022, **157**, 131102.
30 M. J. Hebert and D. H. Russell, *J. Phys. Chem. B*, 2020, **124**, 2081–2087.
31 B. M. Marsh, J. M. Voss and E. Garand, *J. Chem. Phys.*, 2015, **143**, 204201.
32 E. Sato, K. Hirata, J. M. Lisy, S. Ishiuchi and M. Fujii, *J. Phys. Chem. Lett.*, 2021, **12**, 1754–1758.
33 J. A. Stearns, S. Mercier, C. Seaiby, M. Guidi, O. V. Boyarkin and T. R. Rizzo, *J. Am. Chem. Soc.*, 2007, **129**, 11814–11820.
34 E. Garand, M. Z. Kamrath, P. A. Jordan, A. B. Wolk, C. M. Leavitt, A. B. McCoy, S. J. Miller and M. A. Johnson, *Science*, 2012, **335**, 694–698.
35 J. G. Redwine, Z. A. Davis, N. L. Burke, R. A. Oglesbee, S. A. McLuckey and T. S. Zwier, *Int. J. Mass Spectrom.*, 2013, **348**, 9–14.
36 M. Z. Kamrath, E. Garand, P. A. Jordan, C. M. Leavitt, A. B. Wolk, M. J. Van Stipdonk, S. J. Miller and M. A. Johnson, *J. Am. Chem. Soc.*, 2011, **133**, 6440–6448.
37 S. Ishiuchi, H. Wako, D. Kato and M. Fujii, *J. Mol. Spectrosc.*, 2017, **332**, 45–51.
38 W. L. Jorgensen and J. Tirado-Rives, *J. Am. Chem. Soc.*, 1988, **110**, 1657–1666.
39 F. Mohamadi, N. G. J. Richards, W. C. Guida, R. Liskamp, M. Lipton, C. Caufield, G. Chang, T. Hendrickson and W. C. Still, *J. Comput. Chem.*, 1990, **11**, 440–467.
40 M. Frisch, G. Trucks, H. Schlegel, G. Scuseria, M. Robb, J. Cheeseman, G. Scalmani, V. Barone, G. Petersson and H. Nakatsuji, *et al.*, *Gaussian 16*, Gaussian, Inc., Wallingford, CT, 2016.
41 K.-D. Kreuer, A. Rabenau and W. Weppner, *Angew. Chem., Int. Ed. Engl.*, 1982, **21**, 208–209.
42 Y. Matsuda, A. Yamada, K. Hanaue, N. Mikami and A. Fujii, *Angew. Chem., Int. Ed.*, 2010, **49**, 4898–4901.
43 N. Agmon, *Chem. Phys. Lett.*, 1995, **244**, 456–462.
44 M.-P. Gaigeot, A. Cimas, M. Seydou, J.-Y. Kim, S. Lee and J.-P. Schermann, *J. Am. Chem. Soc.*, 2010, **132**, 18067–18077.
45 R. Otsuka, K. Hirata, Y. Sasaki, J. M. Lisy, S. Ishiuchi and M. Fujii, *ChemPhysChem*, 2020, **21**, 712–724.

 